Temperature dependence of the Yb valence in $YbCu_5$ and $YbCu_{5-x}Al_x$ Kondo compounds studied by x-ray spectroscopy

H. Yamaoka,[1] I. Jarrige,[2] N. Tsujii,[3] N. Hiraoka,[4] H. Ishii,[4] and K-D. Tsuei[4]
[1]*Harima Institute, The Institute of Physical and Chemical Research (RIKEN), Sayo, Hyogo 679-5148, Japan*
[2]*Synchrotron Radiation Research Unit, Japan Atomic Energy Agency, 1-1-1 Kouto, Sayo, Hyogo 679-5148, Japan*
[3]*Quantum Beam Center, National Institute for Materials Science, 1-2-1 Sengen, Tsukuba 305-0047, Japan*
[4]*National Synchrotron Radiation Research Center, Hsinchu 30076, Taiwan*
(Received 11 May 2009; revised manuscript received 25 June 2009; published 17 July 2009)

We have performed bulk-sensitive measurements of the temperature dependence of the Yb valence in the hexagonal $YbCu_{5-x}Al_x$ $(0 \leq x \leq 2)$ and cubic $YbCu_5$ Kondo compounds using x-ray absorption spectroscopy in the partial fluorescence yield and resonant x-ray emission spectroscopy. A large difference in the valence is found between the cubic (~2.96) and hexagonal (~2.5) $x=0$ systems, which evidences a strong structural dependence of the Yb electronic properties. For all studied compounds, a temperature dependence of the valence on the order of 0.02 is measured and found consistent with the magnetic susceptibility. This crossover from the low-temperature state having a higher mixed valence to a high-temperature local-moment behavior is analyzed within the Anderson impurity model (AIM). A good agreement is obtained between our data and the AIM. Evidence is brought for valence fluctuation to occur near the quantum critical point at $x=1.5$ and near the antiferromagnetic phase transition at $x=2.0$.

DOI: 10.1103/PhysRevB.80.035120 PACS number(s): 71.20.Eh, 75.30.Mb, 78.70.En, 78.70.Ck

I. INTRODUCTION

Understanding the heavy-fermion state is one of the central challenges in solid-state physics. Enhanced specific heat and magnetic susceptibility are among the low-temperature experimental fingerprints of the heavy-fermion ground state, which was found in some cases to bring about non-Fermi-liquid behavior and unconventional superconductivity.[1] $YbCu_5$-based intermetallic compounds are archetypal heavy-fermion f-electron systems. A wide range of interesting physical phenomena can be spanned upon Cu-site substitution in the hexagonal $YbMCu_4$ systems (M=In, Ag, Au, Cd, Tl, etc.),[2–10] such as temperature-induced valence transition in $YbInCu_4$, Kondo-lattice effects in $YbAgCu_4$, and antiferromagnetic (AF) order in $YbAuCu_4$. In cubic $YbCu_5$, the low-temperature physical properties were described by a Kondo lattice with a heavy Fermi-liquid ground state.[11–17] This rich variety of physical properties seems to stem in large part from the mixed-valence ground state of Yb.[4]

Of particular interest is the Al-substituted system, $YbCu_{5-x}Al_x$, the electronic and magnetic properties of which strongly depend on the Al concentration x.[18–31] The Yb valence increases with x over the 0.5–1.5 range while the Yb^{3+} state is considered to be stable for $x \geq 1.5$. Ensues an interesting evolution of the magnetic behavior; the $x=0$ system is a strongly hybridized Kondo-lattice system with Kondo temperature $T_K \sim 1000$ K, while T_K decreases rapidly to the order of room temperature with increasing x up to 1.0. For $x \geq 1$, T_K is further reduced and the competition between the Kondo and the Ruderman-Kittel-Kasuya-Yosida interactions results in the appearance of long-range antiferromagnetic order with Néel temperature $T_N \sim 1$ K for $x \geq 1.5$. From these results and careful low-temperature transport studies, the concentration $x \sim 1.5$ is regarded to be that of a quantum critical point (QCP), where the system exhibits non-Fermi-liquid properties near incipient magnetism.[24,25] We recently reported on the intermediate-valent character of the $x=1.5$ compound at room temperature and speculated that this mixed-valent behavior is retained even at low temperature near the QCP.[31] In the case where the QCP is in the mixed-valence region, the effect of valence fluctuation can be important for the interpretation of the low-energy excitations at the QCP.[32,33] Nonetheless, in the low-T_K materials the mixed-valent state and its possible effect on the QCP have not been studied so far, mainly because of the small proportion of mixed valence and the weak temperature dependence of the valence. We note that the x dependence of the Yb valence cannot be understood solely in terms of chemical pressure effect.

The Anderson impurity model (AIM) has been widely used to explain the physical phenomena in the region where the Kondo effect and the magnetism compete. The AIM, however, was reported to not account properly for the temperature dependence of the $4f$ occupation number along the crossover from Fermi-liquid ground state to local-moment behavior at high temperature.[4,9,10] Instead, the Anderson lattice model (ALM), or periodic Anderson model, can be used to explain such protracted-screening (slow) crossover.

In this paper we report on the composition and temperature dependencies of the electronic structure of $YbCu_{5-x}Al_x$, using two complementary hard x-ray spectroscopic probes at the Yb L_3 edge, partial fluorescence yield x-ray absorption spectroscopy (PFY-XAS), and resonant x-ray emission spectroscopy (RXES).[31,34–38] For the $x=0$ system, both hexagonal and cubic compounds are studied. In cubic $YbCu_5$, our results are found consistent with a previous thermal-expansion coefficient[5] measurement, and give direct evidence for valence fluctuation. The experimentally derived valences are compared with estimations based on the AIM. The AIM is found to reproduce satisfactorily the normal, fast crossover of the Yb valence (v) with temperature in all the studied systems. These results show that valence fluctuation

occurs even in the vicinity of the QCP for the $x=1.5$ compound and near the AF ordered state of the $x=2.0$ compound.

II. EXPERIMENTS

$YbCu_{5-x}Al_x$ polycrystalline samples were prepared for $x=0$, 0.6, 0.8, 1.0, 1.25, 1.5, and 2.0 by argon arc melting from pure metals and subsequent annealing at 750 °C. The cubic $YbCu_5$ sample was prepared by arc melting and subsequent annealing under high pressure.[11] The melted sample consists of deformed $AuBe_5$-type $YbCu_{4.5}$ and hexagonal $CaCu_5$-type $YbCu_{6/5}$.[11,17] An arc-melted $YbCu_5$ ingot was placed in a boron-nitride cell, which was pressurized to 7 GPa and heated at 900 °C for 2 h. After that, temperature was cooled down to room temperature, at which the pressure was released. The magnetic susceptibility was measured with a superconducting quantum interference device magnetometer at an applied field of 1000 Oe.

PFY-XAS and RXES measurements were performed at the Taiwan beamline BL12XU, SPring-8. The undulator beam was monochromatized by a pair of Si(111) crystals and focused to a size of 120(horizontal) × 80(vertical) μm^2 at the sample position using a toroidal mirror. A Rowland-type spectrometer equipped with a 1 m spherically bent Si(620) crystal was used to analyze the Yb $L\alpha_1(3d_{5/2}\rightarrow 2p_{3/2})$ emission line. The overall energy resolution was about 1.5 eV around the emitted photon energy of 7400 eV. A closed-circuit He cryostat was used for the low-temperature measurements. We note that the use of PFY-XAS has an important advantage to circumvent the strong Cu K absorption which starts ~35 eV above the Yb L_3 edge. The intensities of all spectra are normalized by the incident-beam intensity monitored just before the target.

III. RESULTS AND DISCUSSION

A. Magnetic susceptibility

The temperature dependence of the magnetic susceptibility χ of hexagonal $YbCu_{5-x}Al_x$ ($x=1.5$,1.25,1.5,2.0) and cubic $YbCu_5$ is shown in Figs. 1(a) and 1(b). According to the Bethe-Ansatz solution of the Coqblin-Schrieffer model, the physical properties of a Kondo lattice are well scaled by a single energy parameter (T_0). According to Rajan's model,[39,41] this characteristic temperature is related to the magnetic susceptibility at 0 K $\chi(0)$ by: $\chi(0)T_0=N_A\nu(\nu-1)g_L^2\mu_B^2/(24\pi k_B)$, where N_A is the Avogadro number, ν the ground-state degeneracy, g_L the Landé factor, μ_B the Bohr magnetron, and k_B the Boltzmann constant. We derived the characteristic temperature (T_0) from $\chi(0)$ obtained from previous susceptibility measurements in Ref. 6 by subtracting the Curie-Weiss term due to the impurity at low temperature for $x\leq 1.0$. Using the relation $\chi(0)T_0=3.275$, we obtain $T_0=3280$, 1560, 1370, 480 K for $x=0.6$, 0.7, 0.8, and 1.0, respectively. As increasing x, the characteristic temperature decreases monotonously.

We also estimate the characteristic temperatures for $x\geq 1.0$ by using Rajan's numerical result.[39] As shown in Figs. 1(a) and 1(b), we fit the Rajan's curve to the experimental result of the magnetic susceptibility, making T_0 as a fitting parameter: $T_0=340$, 33, 12, 10, and 67 K for $x=1.0$, 1.25, 1.5, 2.0, and cubic $YbCu_5$, respectively. The theory, however, does not reproduce the temperature dependence of the magnetic susceptibility well.

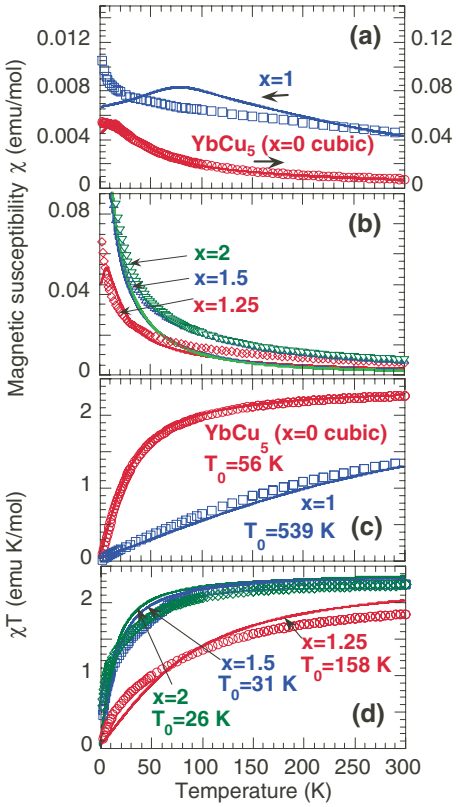

FIG. 1. (Color online) [(a) and (b)] Temperature dependence of the magnetic susceptibility (χ). The solid lines are the fitted curve based on the Rajan's numerical result (Ref. 39); [(c) and (d)] temperature dependence of χT. Solid lines are fitted curves of AIM calculations by Bickers *et al.* (Ref. 40). T_0 is the characteristic temperature derived from the fits.

In Figs. 1(c) and 1(d) we plot the temperature dependence of χT. The solid lines are calculations of the theoretical universal curve based on the AIM by Bickers *et al.*[40] The theoretical fits to the experimental data are not fully satisfactory, indicating that the temperature dependence of the magnetic susceptibility cannot be fully understood within the AIM. Based on those calculations, we estimate the characteristic temperature $T_0=491$, 143, 27, 22, and 51 K for $x=1.0$, 1.25, 1.5, 2.0, and cubic $YbCu_5$, respectively. As will be explained in Sec. III C, we use these characteristic temperatures to fit the temperature dependence of the valence. These values are of the same order as those obtained by Rajan's calculations.

B. Temperature and x dependencies

Figure 2 summarizes the temperature dependence of the Yb L_3 PFY-XAS spectra and Yb $3d_{5/2}2p_{3/2}$-RXES spectra collected at the maximum of the Yb^{2+} resonance ($E_{in}=8934$ eV) for $x=1.5$, 2.0, and cubic $YbCu_5$. The RXES spectra are plotted as a function of the transfer energy, which is defined as the difference between the incident and emitted

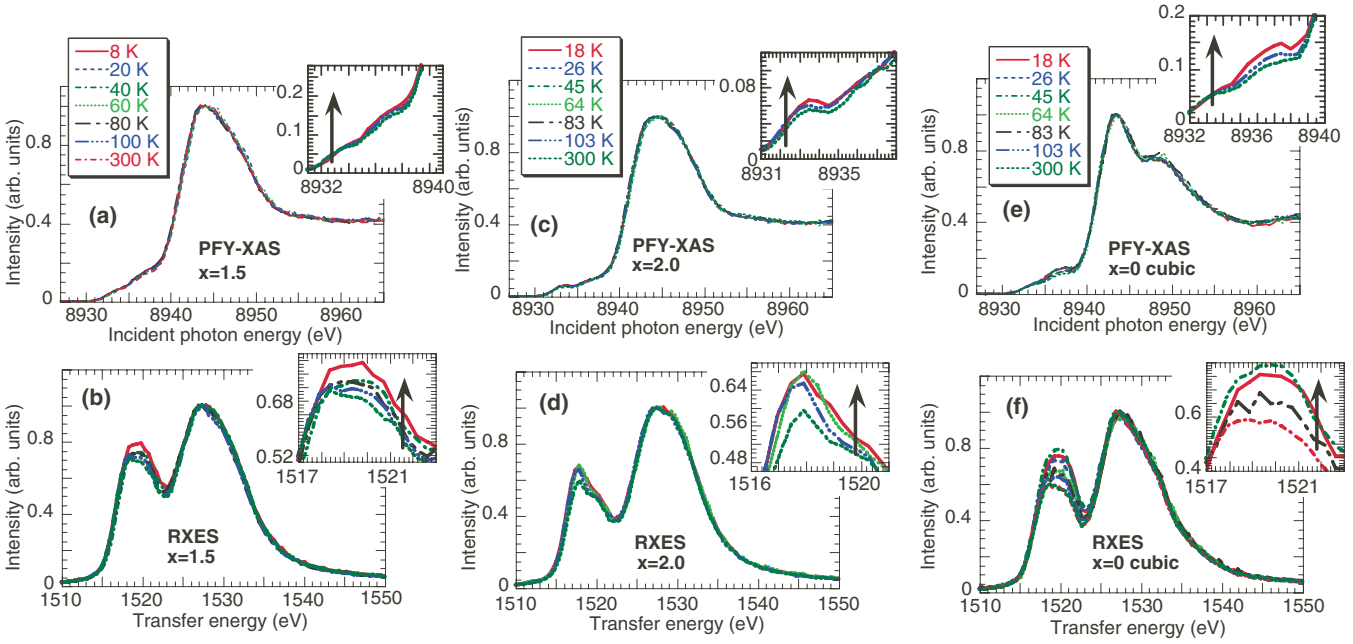

FIG. 2. (Color online) Temperature dependence of the Yb L_3 PFY-XAS and the Yb $3d_{5/2}2p_{3/2}$-RXES (at E_{in}=8934 eV) spectra measured for hexagonal $YbCu_{5-x}Al_x$ (x=1.5,2.0) and cubic $YbCu_5$ (x=0). The inset in each figure is the enlarged 2+ component and arrows in the figures indicate a direction to decrease the temperature.

photon energies. As seen from the enlarged divalent regions of the PFY-XAS and RXES spectra in the insets, the relative intensity of the Yb^{2+} component slightly increases when decreasing temperature. We note that the double-peak structure exhibited by the 3+ component in the PFY-XAS spectrum of cubic $YbCu_5$ [Fig. 2(g)] was attributed by Felner *et al.*[42] to the interaction between the crystal electric field (CEF) and the Yb 5*d* electrons.[38] Oddly enough, this structure in the PFY-XAS, however, is not observed in the hexagonal $YbCu_{5-x}Al_x$ even at low temperature where the effect of the CEF is enhanced.[21]

Figure 3 shows the dependence of the PFY-XAS and RXES spectra upon x at 18 K. The relative intensity of the Yb^{2+} component increases markedly with x. The 2+ peak is found to be much stronger in hexagonal $YbCu_5$ compared with its cubic analogue, revealing strong changes in the electronic structure related to the crystal structure solely. In Fig. 3(c) the change in the intensity of Yb^{2+} is relatively large compared to that of Yb^{3+}. It is noted that in Fig. 3(c) the change in the intensity of Yb^{2+} is relatively large compared to that of Yb^{3+} because the spectra are measured at E_{in} =8934 eV, which corresponds to the Yb^{2+} resonance energy. Accordingly, the Yb^{2+} component is resonantly enhanced, whereas virtually no change can be detected in the Yb^{3+} feature. In Fig. 4 we show examples of the curve fits for the PFY-XAS and RXES at E_{in}=8934 eV, respectively. We subtract arctanlike part to estimate the valence from the PFY-XAS spectra.

We summarize the values of the valence estimated through fitting the PFY-XAS and RXES spectra in Fig. 5(a). Details about the fitting procedures can be found in Refs. 35–38. The data at 300 K are taken from Ref. 31. We note that the RXES at 8934 eV indicates a part of Raman spectra and incident photon energy of 8934 eV is around Yb^{2+} peak in the PFY-XAS spectrum. One can rely on the relative change in the ratio of Yb^{2+} derived from the RXES spectra at the 2+ resonance. We add the fact that in practice in Fig. 5 we use the value of the valence estimated from the PFY-XAS spectra mainly. But in Fig. 5 we also show the values estimated from the RXES at E_{in}=8934 eV because we clearly see relative change in the valence. We also note that if we

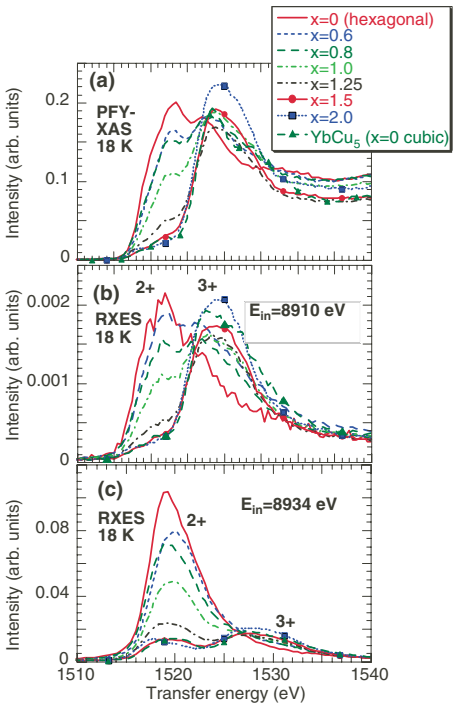

FIG. 3. (Color online) x dependence at 18 K of the Yb L_3 PFY-XAS and the Yb $3d_{5/2}2p_{3/2}$-RXES (E_{in}=8910 and 8934 eV) spectra measured for hexagonal $YbCu_{5-x}Al_x$ and cubic $YbCu_5$.

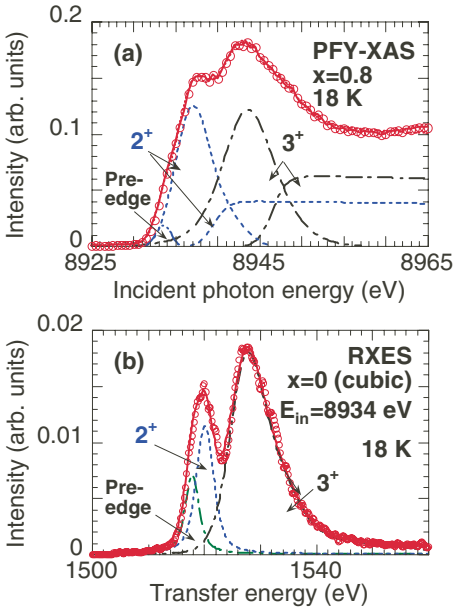

FIG. 4. (Color online) Examples of the curve fits for (a) PFY-XAS of hexagonal $x=0.8$ sample at 18 K and (b) RXES of cubic $x=0$ sample at $E_{in}=8934$ eV and 18 K, respectively. Open circle and solid line correspond to the experimental data and total intensity of fit curves, respectively.

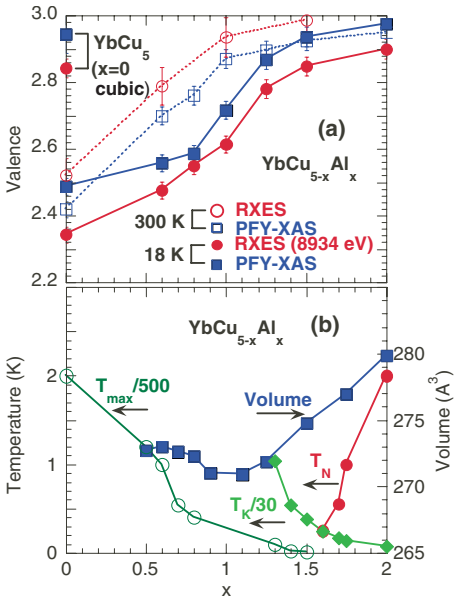

FIG. 5. (Color online) (a) x dependence of the Yb valence. Square and circle symbols correspond to the values derived from the PFY-XAS and RXES, respectively. Closed and open symbols are the measured values at 18 and 300 K, respectively. At $x=0$ the values for cubic $YbCu_5$ at 18 K are also shown. Note that the RXES data at 18 K show measurement at $E_{in}=8934$ eV while those at 300 K were the curve-fit result for that as a function of temperature. (b) x dependence of Kondo temperature (T_K, closed diamond), Néel temperature (T_N, closed square), maximum temperature of magnetic susceptibility (T_{max}, open circle), and volume (closed circle) are shown, where the values of T_K and T_{max} are divided by a factor of 500 and 30, respectively (Refs. 6, 22, 24, 25, 43, and 44).

adjust the valence obtained from RXES at 8934 eV to that of PFY at $x=0$, where Yb^{2+} is dominant, the agreement between the PFY-XAS and RXES at 8934 eV becomes better. The variation in the valence derived from RXES is put on an absolute scale by using the value of the valence obtained from the PFY-XAS spectrum for $x=2$. The two techniques of the PFY-XAS and RXES at $E_{in}=8934$ eV show the same trend, which further substantiates the reliability of our analytical method. While at both 300 and 18 K the valence decreases continuously with x, at 18 K a steeper variation is found over the 0.8–1.25 range. This difference could be explained by the idea of Bauer *et al.*[22] that for $x=0.75-1.0$ the energy difference between the Yb^{3+} and Yb^{2+} states is of the order of the thermal excitation energy, whereas for $x \geq 1.5$ it is much larger and no temperature dependence is expected. We note that our results at 300 K are in good agreement with those of Bauer *et al.*[22] In Fig. 5(b) we show the dependence in x of the Kondo temperature (T_K), the Néel temperature (T_N), maximum temperature of magnetic susceptibility (T_{max}), and the volume. These data are taken from Refs. 6, 22, 24, 25, 43, and 44.

Besides the overall volume increase upon Al substitution, a slight volume decrease is observed between $x=0.5$ and $x=1$ as shown in Fig. 5(b).[44] This appears to coincide with the rapid increase in v in the same x range, the radius of Yb^{3+} being smaller than that of Yb^{2+}. This v increase stems from the increase in the number of conduction electrons and decrease in Cu $3d$ density of states (DOS) (Ref. 45) with increasing Al content, and therefore in a weaker mixing between the $4f$ and conduction states. This may lead to a weakening of the Kondo interactions, as seen from the concomitant decrease in the T_K, which in turns results in the onset of long-range magnetic order at $x \geq 1.5$.

As observed in Fig. 5(a), the valence decreases with temperature. This gives further credence to the speculation we made in Ref. 31 that charge fluctuations would coexist with the QCP at $x \sim 1.5$ and 0 K. We note that such occurrence of charge fluctuations at the QCP was suggested in recent ALM calculations[32] to yield a spin-liquid phase.

C. Comparison with the AIM models

Figure 6 shows the temperature dependence of v for $x=0$ (cubic), 1.5, 2, with the AIM fits. Small changes in the valence, on the order of 0.02, are systematically observed upon cooling, and the most notable changes occur below 100 K. They correspond to the crossover from low-temperature mixed-valent state to high-temperature local-moment behavior. We note these changes are substantially weaker than those previously reported for $YbCu_{5-x}Ag_x$, on the order of 0.05.[5] This is consistent with the AIM prediction that only a small change in the valence occurs above T_K in low-T_K systems.

The AIM does not have an exact solution for $n_f \neq 1$, where n_f is the f occupation number defined as $v=2+n_f$. This can be circumvented by using the noncrossing approximation,[40] for which the temperature dependence of the valence follows the equation: $v(T)=2+n_f(\infty) - [\Delta n_f(T)/\Delta n_f(0)]\Delta n_f(0)$, where $n_f(\infty)$ and $\Delta n_f(T)$ are inter-

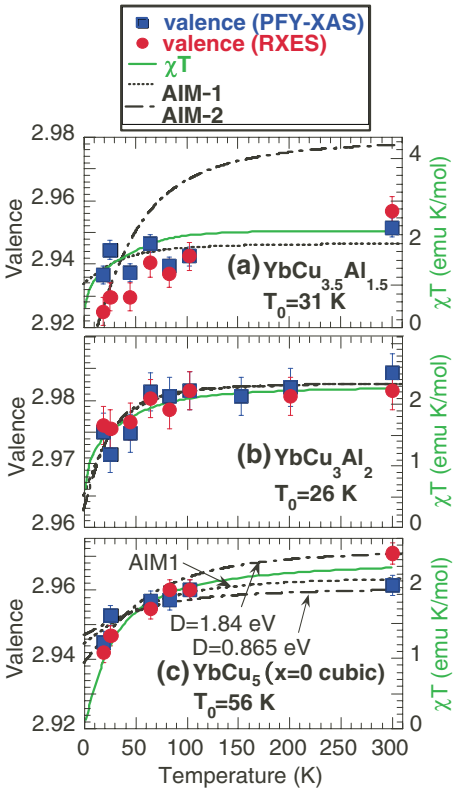

FIG. 6. (Color online) Summarized results of the temperature dependence of the valence for (a) hexagonal $YbCu_{3.5}Al_{1.5}$ ($x=1.5$), (b) hexagonal $YbCu_3Al_2$ ($x=2.0$), and (c) cubic $YbCu_5$. Closed square and closed circle symbols correspond to the values derived from the fits for PFY and RXES, respectively. The fits based on the AIM calculations are shown as dashed line for the valence (AIM-1: dashed line and AIM-2: dashed-dotted line). The temperature dependence of χT is also shown along with the AIM fit (solid line).

mediate temperature limit of the valence and total decrease in valence, respectively. $\Delta n_f(T)/\Delta n_f(0)$ was calculated as a function of T/T_0. We analyze the temperature dependence of the valence derived by PFY-XAS using two fitting techniques, which will be referred to as AIM-1 and AIM-2 hereafter. In the fits we used T_0 estimated from the curve fit for the magnetic-susceptibility measurements in Fig. 1. In the AIM-1 fit $n_f(\infty)$ and $\Delta n_f(0)$ are free parameters. Comparatively, the AIM-2 fit is more quantitative; only $\Delta n_f(0)$ is free parameter and $n_f(\infty)$ is fixed to the values deduced from the conduction bandwidth D of La- or Lu-based nonmagnetic reference compounds, D being inferred from the experimental electronic specific-heat coefficient γ (see Appendix for details). The parameters used in and derived from the model calculations are summarized in Table I.

The AIM-1 is seen in Fig. 6 to reproduce the temperature dependence of v for all three compounds within the error bars. We note that a similar fitting technique has been previously applied to $YbXCu_4$ (X=Ag, Au, Cd, Mg, Tl, and Zn) but failed to reproduce quantitatively the experimental results as physically unreasonable values of D were obtained.[4] Interestingly, in our case the deduced D values are physically reasonable and the estimated values of $n_f(\infty)$ are nearly 1 and agree well with the experimental ones (cf. Table I). This good agreement indicates that a simple qualitative approach such as the AIM, based on a parameter extracted from the experimental magnetic susceptibility (T_0), is valid even for systems that show a QCP or AF order. Importantly, this provides sound evidence for valence fluctuation to occur in the vicinity of the QCP at $x=1.5$ and near the AF phase transition at $x=2.0$. Indeed, from the single observation of the two peaks related to the 2+ and 3+ states in the absorption spectrum, it would not have been possible to distinguish between valence fluctuation and inhomogeneous mixed valence.

While an excellent agreement is obtained for the AIM-2 fit of $YbCu_3Al_2$ and cubic $YbCu_5$, a deviation up to 2% is found in the high-temperature range of $YbCu_{3.5}Al_{1.5}$. Let us review the possible reasons for this slight discrepancy. Firstly, it could stem from the almost similar values of T_0 estimated for $x=1.5$ and $x=2.0$ (cf. Sec. III A), in spite of the higher valence of $x=1.5$. The estimated T_0 could be subject to inaccurateness because of the large CEF in these compounds [~100 K for $YbCu_3Al_2$ (Ref. 21)] which is not taken into account in the present model. Secondly, there is no measurement yet reported of the specific heat γ of

TABLE I. Input and derived parameters in the model calculations of Figs. 1 and 5. The characteristic temperature T_0 is the derived values from the AIM fit for magnetic susceptibility in Fig. 1. In the fit of AIM-1 intermediate temperature limit of the valence $n_f(\infty)$ and total decrease in valence Δn_f are fit parameters. In AIM-2 γ and conduction-electron bandwidth D are given and only Δn_f is fit parameter.

					AIM-1			AIM-2			
x	T_K (K)	T_{coh} (K)	T_N (K)	T_0 (K)	$n_f(\infty)$	Δn_f	D (eV)	γ (mJ/mol K^2)	D (eV)	$n_f(\infty)$	Δn_f
1.0				5391							
1.25				158							
1.5	11.6[a]			31	0.946	0.025	0.41	6.5[f]	3.71	0.980	0.146
2.0	2.4[a]		2.0[b]	26	0.983	0.035	6.2	4[d]	6.57	0.983	0.035
Cubic $YbCu_5$	60[c]	6[c]		56	0.964	0.038	1.0	9.5[e]	0.865[f]	0.960	0.027
								9.5[e]	1.84	0.972	0.065

[a]Reference 25.
[b]Reference 22.
[c]Reference 3.
[d]Reference 46.
[e]Reference 47.
[f]Reference 10.

$LaCu_{3.5}Al_{1.5}$, which we need in order to calculate the bandwidth D. We assumed a linear interpolation between the γ of $LaCu_5$(14 mJ/mol K^2) and $LaCu_3Al_2$(4 mJ/mol K^2), thus estimating γ=6.5 mJ/mol K^2 for $LaCu_{3.5}Al_{1.5}$. This assumption is another possible source of error. Furthermore, we note that the x dependence of v between 1.0 and 1.5 is abrupt, stemming from a drastic growth in the Cu 3d-Yb 4f hybridization upon substitution of Al with Cu.[45] Accordingly, another limitation of the model comes from the use of a simple Gaussian line shape for the DOS of $YbCu_{5-x}Al_x$ (cf. Appendix).

As the observation of valence fluctuation near the QCP could be thought of as a signature of the Anderson lattice behavior, we turn now to the possibility of employing the ALM to interpret our data. Dynamical mean-field calculation with the ALM by Tahvildar-Zadeh *et al.*[48,49] showed that for $n_d \ll n_f$ (n_d is the conduction-band filling) the Kondo scale is strongly suppressed and the temperature dependence of the Kondo screening is protracted (slow crossover) while for $n_d \sim n_f \sim 1$ it is contracted (fast crossover). An important difference between the AIM and the ALM is that slow crossovers are not properly accounted for by the former one, whereas only small differences exist between the two models at $n_d \approx n_f \approx 1$. In order to assess whether the use of ALM could be relevant to our systems, we need to consider the energy scale relevant to the ALM, the coherence temperature T_{coh}, defined as $k_B T_{coh} = \rho(1-n_{fh})V^2$, where ρ, n_{fh}, and V are the conduction-band DOS, the number of holes in the f shell and the hybridization strength, respectively.[50–52] Below T_{coh}, the system is in a Fermi-liquid state. In $YbCu_{5-x}Al_x$, the ground state is magnetic for x=1.5,[25,31] and the QCP occurs at T=0 K in x=2.0,[25] so that neither of these systems exhibits a Fermi-liquid ground state. Based on this consideration, the applicability of the ALM to $YbCu_{5-x}Al_x$ can be ruled out.

Finally we note that the change in the valence follows closely the temperature dependence of χT, as was already observed in other Yb materials.[38] The decrease in χT with temperature stems from the concomitant decrease in the magnetic Yb^{3+} component, Yb^{2+} being nonmagnetic.

D. RXES for $YbCu_5$

The RXES spectra measured on $YbCu_5$ at 18 K as a function of the incident energy across the Yb L_3 edge are shown in Fig. 7(b). The vertical offset of the RXES spectra corresponds to the incident energy in panel (a) which they were collected at. Going from low- to high-incident photon energy, one can successively observe the Raman regime where the signal remains at constant transfer energy, progressively evolving into the fluorescence which shifts toward high transfer energies. Each spectrum is fitted with three components corresponding to the Raman 2+ and 3+ and the fluorescence. The incident energy dependence of the intensity of these respective components is displayed in Fig. 7(c). From this fit, the Yb valence is estimated to be 2.96, which agrees well with the value derived from PFY-XAS. The lattice constant of cubic $YbCu_5$ is 6.975 Å, much larger than that of its hexagonal counterpart (a=4.993 Å and b=4.216 Å).[19,25] The larger lattice constant brings about a lower mixing between the 4f electrons and the conduction states, causing both a departure from the mixed-valence characteristic of the hexagonal system, and an increase in the magnetic moment as shown in Fig. 1.

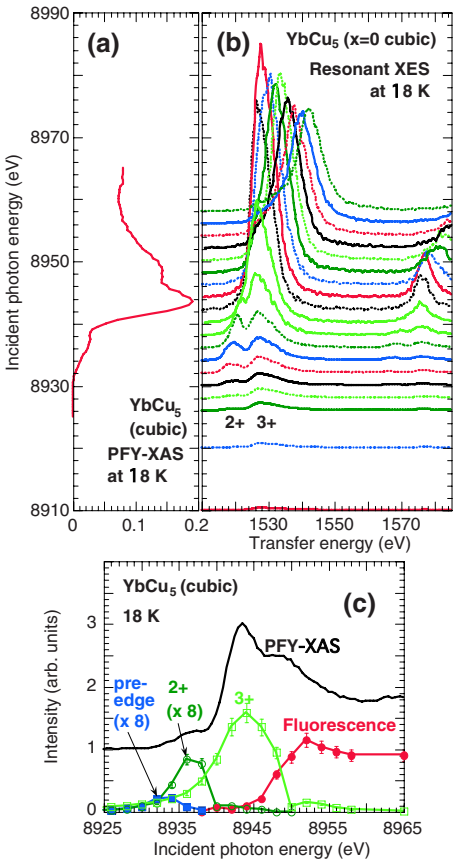

FIG. 7. (Color online) Yb $2p_{3/2}-3d_{5/2}$ RXES spectra obtained for several values of E_{in} across the L_3 edge on $YbCu_5$ at 18 K. The vertical position of the RXES spectra in panel (b) corresponds to the E_{in} they were measured at in panel (a). The E_{in} dependence of the respective components fitted in the RXES spectra is shown in (c). 2+ (open circle), 3+ (open square), fluorescence (closed circle), and pre-edge (closed square) components are shown, respectively, with the PFY-XAS.

IV. CONCLUSION

We performed a bulk-sensitive x-ray spectroscopic study of the temperature and x dependencies of the electronic structure of hexagonal $YbCu_{5-x}Al_x$ ($0 \le x \le 2$) system and cubic $YbCu_5$ Kondo compound by using x-ray absorption spectroscopy in the partial fluorescence yield and resonant x-ray emission spectroscopy. The valence of hexagonal and cubic $YbCu_5$ is nearly 2.5 and 3, respectively, indicating a strong structure dependence of the electronic states in spite of an identical chemical formula. Our measurements show that the Yb^{3+} state is favored in the hexagonal $YbCu_{5-x}Al_x$ compounds with large x and cubic $YbCu_5$, and accordingly magnetic ordering sets in. On the other hand, lower values of x are characterized by both strong mixed valence and Kondo effect. We succeeded to observe a small change in the va-

lence as a function of the temperature, showing a crossover from localized Yb^{3+} weak mixed valence to intermediate valence as decreasing the temperature for both hexagonal $YbCu_{5-x}Al_x$ ($x=1.5$ and 2.0) and cubic $YbCu_5$ systems. The valence shows a rapid decrease in small amplitude (~ 0.02) with temperature below 100 K for the three measured systems ($x=1.5$, 2, and 0 cubic), following closely the temperature dependence of χT. The good agreement between the theory based on the Anderson impurity model and the temperature dependence of v indicates that the AIM is valid for describing the crossovers in Yb Kondo materials with low T_K. Interestingly, mixed valence is observed in the vicinity of the quantum critical point at $x=1.5$, where the low-temperature ground state is antiferromagnetic, and the valence is nonintegral. This indicates that the QCP divides the nonmagnetic regime from the antiferromagnetic regime, occurring within a weakly mixed-valent state. This also raises a possibility that valence fluctuations may play a role in the behavior near the QCP, rather hinting to an AL behavior, although the ALM model is not applicable to our systems.

ACKNOWLEDGMENTS

The experiments were performed at Taiwan beamline BL12XU (SPring-8 under Proposal No. 2008A4255 and NSRRC under Project No. 2008-2-015-1) at SPring-8. We appreciate Hiroya Sakurai of NIMS for his help in preparing the cubic $YbCu_5$ sample. This work was supported by a Grant-in-Aid for Scientific Research No. 19740221 from the Ministry of Education, Culture, Sports, Science and Technology of Japan.

APPENDIX

$n_f(\infty)$ is related to the bandwidth D of the conduction-electron band without $c-f$ hybridization,[4,10] it can be deduced from the γ of $LaCu_{5-x}Al_x$ (Refs. 46 and 53) or $LuCu_5$,[47] which are isostructural with $YbCu_{5-x}Al_x$ and cubic $YbCu_5$, respectively. We deduce the D according to the relations: $\gamma(\varepsilon_f)=\pi^2 k_B^2 N(\varepsilon_f)/3=[\pi^2 k_B^2/3][2n_e N_A \exp(-\varepsilon_f^2/W^2)]$ and thus $D=(\ln 2)^{1/2}W=2.190 n_e/\gamma(0)$, where $N(\varepsilon_f)$, n_e, and W are DOS at Fermi level, number of valence electrons, and Gaussian DOS width, respectively. For cubic $YbCu_5$, $D=0.865$ eV in $YbAgCu_4$ derived by Lawrence *et al.* is also used for comparison.[10] In the AIM-2 fit we used the relation between $g=1-n_f(\infty)$ and D in Table I of Ref. 40 for Ce system ($J=5/2, \nu=6$) because the degeneracy may decrease due to the crystal-field effect as described before. It is noted that D changes in a log scale when $g=1-n_f(\infty)$ is changed in a linear scale.

[1] N. D. Mathur, F. M. Grosche, S. R. Julian, I. R. Walker, D. M. Freye, R. K. W. Haselwimmer, and G. G. Lonzarich, Nature (London) **394**, 39 (1998).
[2] E. Bauer, Adv. Phys. **40**, 417 (1991).
[3] N. Tsujii, J. He, K. Yoshimura, K. Kosuge, H. Michor, K. Kreiner, and G. Hilscher, Phys. Rev. B **55**, 1032 (1997).
[4] J. L. Sarrao, C. D. Immer, Z. Fisk, C. H. Booth, E. Figueroa, J. M. Lawrence, R. Modler, A. L. Cornelius, M. F. Hundley, G. H. Kwei, J. D. Thompson, and F. Bridges, Phys. Rev. B **59**, 6855 (1999).
[5] E. R. Hauser, K. Kreiner, E. Bauer, H. Michor, G. Hilscher, M. Rotter, H. Muller, N. Tsujii, K. Yoshimura, and K. Kosuge, Physica B **259-261**, 136 (1999).
[6] K. Yoshimura, N. Tsujii, J. He, and K. Kosuge, JJAP Ser. **8**, 363 (1999).
[7] N. Tsujii, T. Terashima, C. Terakura, G. Kido, T. Kawabata, K. Yoshimura, and K. Kosuge, J. Phys.: Condens. Matter **13**, 3623 (2001).
[8] V. A. Shaburov, A. E. Sovestnov, Yu P. Smirnov, A. V. Tyunis, and A. V. Golubkov, Phys. Solid State **43**, 1420 (2001).
[9] J. M. Lawrence, G. H. Kwei, P. C. Canfield, J. G. DeWitt, and A. C. Lawson, Phys. Rev. B **49**, 1627 (1994).
[10] J. M. Lawrence, P. S. Riseborough, C. H. Booth, J. L. Sarrao, J. D. Thompson, and R. Osborn, Phys. Rev. B **63**, 054427 (2001).
[11] N. Tsujii, J. He, F. Amita, K. Yoshimura, K. Kosuge, H. Michor, G. Hilscher, and T. Goto, Phys. Rev. B **56**, 8103 (1997).
[12] N. Tsujii, K. Yoshimura, and K. Kosuge, Phys. Rev. B **59**, 11813 (1999).
[13] K. Yoshimura, N. Tsujii, K. Sorada, T. Kawabata, H. Mitamura, T. Goto, and K. Kosuge, Physica B **281-282**, 141 (2000).
[14] M. Reiffers, B. Idzikowski, S. Ilkovič, A. Zorkovská, J. Šebek, and K. H. Mŏller, J. Magn. Magn. Mater. **272-276**, 209 (2004).
[15] M. Reiffers, B. Idzikowski, J. Šebek, E. Šantavá, S. Ilkovič, and G. Pristáš, Physica B **378-380**, 738 (2006).
[16] T. Mito, M. Nakamura, M. Shimoide, M. Otani, T. Koyama, S. Wada, H. Kotegawa, T. C. Kobarashi, B. Idzikowski, M. Reiffers, and J. L. Sarrao, Physica B **378-380**, 732 (2006).
[17] M. Giovannini, R. Pasero, S. De Negri, and A. Saccone, Intermetallics **16**, 399 (2008).
[18] E. Bauer, K. Payer, R. Hauser, E. Gratz, D. Gignoux, D. Schmitt, N. Pillmayr, and G. Schaudy, J. Magn. Magn. Mater. **104-107**, 651 (1992).
[19] E. Bauer, R. Hauser, E. Gratz, D. Gignoux, D. Schmitt, and J. Sereni, J. Phys.: Condens. Matter **4**, 7829 (1992).
[20] E. Bauer, E. Gratz, L. Keller, P. Fisher, and A. Furrer, Physica B **186-188**, 608 (1993).
[21] P. Bonville and E. Bauer, J. Phys.: Condens. Matter **8**, 7792 (1996).
[22] E. Bauer, R. Hauser, L. Keller, P. Fischer, O. Trovarelli, J. G. Sereni, J. J. Rieger, and G. R. Stewart, Phys. Rev. B **56**, 711 (1997).
[23] J. He, N. Tsujii, K. Yoshimura, and K. Kosuge, J. Alloys Compd. **268**, 221 (1998).
[24] E. Bauer, R. Hauser, A. Galatanu, H. Michor, G. Hilscher, J. Sereni, M. G. Berisso, P. Pedrazzini, M. Galli, F. Marabelli, and P. Bonville, Phys. Rev. B **60**, 1238 (1999).
[25] P. Bonville, E. Vincent, and E. Bauer, Eur. Phys. J. B **8**, 363 (1999).
[26] C. Seuring, K. Heuser, E.-W. Scheidt, T. Schreiner, E. Bauer, and G. R. Stewart, Physica B **281-282**, 374 (2000).

[27] E. Bauer, A. Galatanu, L. Naber, M. Galli, F. Marabelli, C. Seuring, K. Heuser, E.-W. Scheidt, T. Schreiner, and G. R. Stewart, Physica B **281-282**, 319 (2000).
[28] N. Tsujii, H. Mitamura, T. Goto, K. Yoshimura, K. Kosuge, T. Terashima, T. Takamasu, H. Kitazawa, S. Kato, and G. Kido, Physica B **294-295**, 284 (2001).
[29] C. Seuring, E.-W. Scheidt, E. Bauer, and G. R. Stewart, J. Low Temp. Phys. **123**, 25 (2001).
[30] G. Pristáš, M. Reiffers, and E. Bauer, Physica B **378-380**, 100 (2006).
[31] K. Yamamoto, H. Yamaoka, N. Tsujii, A. M. Vlaicu, H. Oohashi, S. Sakakura, T. Tochio, Y. Ito, A. Chainani, and S. Shin, J. Phys. Soc. Jpn. **76**, 124705 (2007).
[32] C. Pepin, Phys. Rev. Lett. **98**, 206401 (2007).
[33] P. Gegenwart, Q. Si, and F. Steglich, Nat. Phys. **4**, 186 (2008), and references therein.
[34] I. Jarrige, H. Ishii, Y. Q. Cai, J.-P. Rueff, C. Bonnelle, T. Matsumura, and S. R. Shieh, Phys. Rev. B **72**, 075122 (2005).
[35] H. Yamaoka, M. Taguchi, A. M. Vlaicu, H. Oohashi, Y. Yokoi, D. Horiguchi, T. Tochio, Y. Ito, K. Kawatsura, K. Yamamoto, A. Chainani, S. Shin, M. Shiga, and H. Wada, J. Phys. Soc. Jpn. **75**, 034702 (2006).
[36] H. Yamaoka, N. Tsujii, K. Yamamoto, H. Oohashi, A. M. Vlaicu, K. Kunitani, K. Uotani, D. Horiguchi, T. Tochio, Y. Ito, and S. Shin, Phys. Rev. B **76**, 075130 (2007).
[37] H. Yamaoka, H. Oohashi, I. Jarrige, T. Terashima, Y. Zou, H. Mizota, S. Sakakura, T. Tochio, Y. Ito, E. Ya. Sherman, and A. Kotani, Phys. Rev. B **77**, 045135 (2008).
[38] H. Yamaoka, N. Tsujii, K. Yamamoto, A. M. Vlaicu, H. Oohashi, H. Yoshikawa, T. Tochio, Y. Ito, A. Chainani, and S. Shin, Phys. Rev. B **78**, 045127 (2008).
[39] V. T. Rajan, Phys. Rev. Lett. **51**, 308 (1983).
[40] N. E. Bickers, D. L. Cox, and J. W. Wilkins, Phys. Rev. B **36**, 2036 (1987).
[41] B. Coqblin and J. R. Schriffer, Phys. Rev. **185**, 847 (1969).
[42] I. Felner, I. Nowik, D. Vaknin, U. Potzel, J. Moser, G. M. Kalvius, G. Wortmann, G. Schmiester, G. Hilscher, E. Gratz, C. Schmitzer, N. Pillmayr, K. G. Prasad, H. de Waard, and H. Pinto, Phys. Rev. B **35**, 6956 (1987).
[43] K. Yoshimura, N. Tsujii, J. He, T. Kawabata, H. Michor, K. Kreiner, G. Hilscher, T. Miyano, M. Kato, and K. Kosuge, Mater. Struct. Chem., Biol., Phys. Technol. **5**, 245 (1998).
[44] J. He, Ph.D. thesis, Division of Chem., Graduate School of Science, Kyoto University, 1999; J. He, G. Ling, and Z. Ye, J. Alloys Compd. **325**, 54 (2001).
[45] K. Yamamoto, M. Matsunami, M. Taguchi, K. Horiba, R. Eguchi, T. Takeuchi, Y. Takata, A. Chainani, K. Mimura, D. Miwa, Y. Nishino, K. Tamasaku, M. Yabashi, T. Ishikawa, Y. Senba, H. Ohashi, N. Tsujii, and S. Shin (unpublished).
[46] D. P. Rojas, L. P. Cardoso, A. A. Coelho, F. G. Gandra, and A. N. Medina, Phys. Rev. B **63**, 165114 (2001).
[47] H. Michor, K. Kreiner, N. Tsujii, K. Yoshimura, K. Kosuge, and G. Hilscher, Physica B **319**, 277 (2002).
[48] A. N. Tahvildar-Zadeh, M. Jarrell, and J. K. Freericks, Phys. Rev. B **55**, R3332 (1997).
[49] A. N. Tahvildar-Zadeh, M. Jarrell, and J. K. Freericks, Phys. Rev. Lett. **80**, 5168 (1998).
[50] A. L. Cornelius, J. M. Lawrence, T. Ebihara, P. S. Riseborough, C. H. Booth, M. F. Hundley, P. G. Pagliuso, J. L. Sarrao, J. D. Thompson, M. H. Jung, A. H. Lacerda, and G. H. Kwei, Phys. Rev. Lett. **88**, 117201 (2002).
[51] S. Burdin, D. R. Grempel, and A. Georges, Phys. Rev. B **66**, 045111 (2002).
[52] S. Burdin and P. Fulde, Phys. Rev. B **76**, 104425 (2007).
[53] P. Svoboda, M. Diviš, J. Bischof, Z. Smetana, R. Černý, and J. Buriánek, Phys. Status Solidi A **119**, K67 (1990).